npj | soft matter

Article

https://doi.org/10.1038/s44431-025-00015-4

Quadrupolar gyration of a Brownian particle in a confining ring

Check for updates

Iman Abdoli ✉ & Hartmut Löwen

We develop a minimal theoretical model that reveals a structured steady-state flux field with four alternating local circulation, a phenomenon we refer to as *quadrupolar gyration*. A passive Brownian particle is confined to move in a ring-shaped trap and driven far from equilibrium solely by anisotropic thermal fluctuations from two orthogonal heat baths held at different temperatures. By breaking detailed balance, this fundamental temperature anisotropy induces a robust nonequilibrium steady state characterized by probability currents of the particle's motion. Remarkably, these currents self-organize into a distinctive quadrupolar vortex pattern, providing a clear signature of emergent symmetry breaking, irreversible entropy production, and coherent motion in minimal passive systems. Our theoretical predictions, based on the narrow-ring approximation and the assumption of small thermal anisotropy, are validated by numerical simulations.

Brownian gyrator is a minimal microscopic system that elegantly demonstrates how thermal anisotropy—where the particle's orthogonal spatial degrees of freedom are coupled to heat baths at unequal temperatures—can inherently generate steady-state rotational fluxes without external forces or torques[1–7]. Originally conceived as a nanoscale heat engine consisting of a particle diffusing in a two-dimensional anisotropic harmonic potential with misaligned principal axes relative to temperature axes, the Brownian gyrator transforms thermal noise from orthogonal heat baths into persistent probability currents, exemplifying symmetry breaking and directed motion in microscopic systems[8–12]. This mechanism has since emerged as a fundamental model system for probing its electrical counterpart, universal trade-offs governing nonequilibrium engines[13,14] and for studying inertia effect, trajectory-level fluctuations, and entropy production through stochastic thermodynamic tools[15–18]. The gyrator has also been reinterpreted as a minimal information engine, where work extraction is viewed as internal information flow, akin to a Maxwell demon[19].

The emergence of gyrating motion crucially depends on spatial cross-correlations, which can be originated internally from potential structures or externally from magnetic fields[20–23]. Recent work reveals nonharmonic double-well potentials induce counter-rotating fluxes near minima, highlighting geometry's control over nonequilibrium current patterns[24,25]. The theoretical predictions of a Brownian gyrator have been realized in experiments by emulating anisotropic thermal noise via strongly fluctuating electric fields applied along one direction, effectively mimicking the role of additional temperature[26]. The efficiency of an engine relies sensitively on how external mechanical loads, such as shear forces, are applied and tuned to extract work from the engine[27].

Unlike the conventional two-dimensional anisotropic harmonic potential—where misaligned principal axes drive dynamics—a ring-shaped confinement imposes radical geometric restrictions, pinning particles to a fixed radius while enabling free angular diffusion. This transforms the system's essential character from planar stochastic motion to quasi-one-dimensional gyration governed by curvature and confinement. In this geometry, the particle's motion becomes predominantly angular, and any remaining radial diffusion is tightly suppressed. This shift introduces qualitatively different modes of flux formation. Consequently, the ring trap provides a minimalistic and highly controllable platform for investigating nonequilibrium steady states driven by anisotropic fluctuations, and highlights opportunities to explore the roles of spatial geometry and thermal noise in generating rotational probability currents.

Optical ring traps have enabled the controlled realization of persistent circulating currents, noise rectification, and symmetry breaking under anisotropic driving[28–30]. Recent experiments on optically confined colloids have demonstrated that temperature gradients can drive sustained particle transport via optothermal hydrodynamic coupling, elucidating how ring geometries mediate collective phenomena such as unidirectional circulation and spontaneous vortex formation[31]. Theoretical studies have examined Brownian motion on a ring in diverse contexts, including winding statistics[32], stochastic resetting[33], and large deviation theory[34]. In active matter, confined self-propelled particles exhibit curvature-sensitive accumulation and current reversal[35], highlighting the geometric control of transport in driven systems.

Here we study a paradigmatic stochastic system: a Brownian particle confined to a narrow ring and coupled to two orthogonal heat baths at unequal temperatures. The resulting interplay between thermal anisotropy and geometric curvature drives the emergence of steady-state probability currents and entropy production, even in the absence of external forces or torques. Remarkably, we find that the system spontaneously generates a

Institut für Theoretische Physik II - Weiche Materie, Heinrich-Heine-Universität Düsseldorf, Düsseldorf, Germany. ✉e-mail: iman.abdoli@hhu.de

steady-state flux field with four alternating vortical sectors, forming a robust pattern that we term *quadrupolar gyration*. These nonequilibrium features are captured analytically via a perturbative solution of the Fokker-Planck equation in the narrow-ring limit, and validated by direct numerical simulations. We compute the full spatial structure of the steady-state probability distribution, probability currents, and entropy production density, and reveal how their topology and intensity depend sensitively on the noise anisotropy and ring radius.

Results

Model and setup

We consider a Brownian particle restricted to move in a narrow ring-shaped confinement, subjected to anisotropic thermal fluctuations. The particle resides in a two-dimensional plane and experiences independent noise sources with distinct temperatures T_x and T_y along the orthogonal Cartesian axes x and y (see Fig. 1). Unlike conventional Brownian gyrators confined in planar harmonic wells, here the particle is radially confined to a circular shell of radius R, effectively reducing the accessible degrees of freedom to quasi-one-dimensional motion along the angular direction. This geometry eliminates the possibility of global translation or drift, isolating rotational degrees of freedom and enabling clear observation of emergent circulating currents.

The confinement is modeled by a radial potential of the form

$$U(r) = \frac{k}{2}(r - R)^2, \tag{1}$$

which restricts fluctuations around the mean radius R with stiffness k and distance $r = \sqrt{x^2 + y^2}$, while allowing free diffusion in the azimuthal direction.

To analyze the system, we derive the corresponding Fokker-Planck equation in polar coordinates and study the emergence of steady-state solutions under the narrow-ring approximation, $\sqrt{T_x/k} \ll R$, where radial confinement is tight but finite. The probability density $P(r, \theta, t)$ evolves according to the Fokker–Planck equation, expressed in compact tensorial form as (see Supplementary Material (SM))

$$\frac{\partial P}{\partial t} = -\nabla \cdot \left[\mu \mathbf{F} P - \mathbf{D}(\theta) \cdot \nabla P\right], \tag{2}$$

where $\mathbf{F} = -\nabla U(r) = -k(r - R)\hat{\mathbf{e}}_r$ is the radial restoring force derived from the ring-shaped potential. As we derive in the SM, the diffusion coefficient picks up a tensorial form in polar basis which reads

$$\mathbf{D}(\theta) = \mu T \begin{pmatrix} 1 - \alpha \cos 2\theta & \alpha \sin 2\theta \\ \alpha \sin 2\theta & 1 + \alpha \cos 2\theta \end{pmatrix}. \tag{3}$$

Here, $\mu = \gamma^{-1}$ is the mobility with γ being the friction coefficient, $\alpha = (\beta - 1)/(\beta + 1)$ is the dimensionless anisotropy parameter and $T = T_x(\beta + 1)/2$ is the mean effective temperature with $\beta = T_y/T_x$ where $\beta = 1$ corresponds to the isotropic system. We set the Boltzmann constant k_B to unity throughout this work.

The Fokker-Planck equation is derived directly from the system's Itô Langevin equations in Cartesian coordinates, where the noise is additive and no ambiguity in the stochastic calculus exists. The transformation to polar coordinates is performed at the level of the Fokker-Planck equation[36], a well-defined procedure that automatically incorporates all geometric contributions through the divergence operator in Eq. (2), yielding the correct diffusion tensor, Eq. (3). This approach bypasses the need for a spurious drift correction that can arise when transforming the Langevin equations directly[37].

Potential experimental realization

A potential experimental realization of a ring-constrained Brownian gyrator can be achieved by combining a *ring-shaped optical trap*, as implemented by Chand et al.[31], with the *anisotropic thermal noise generation technique* developed by Volpe et al.[26]. The system consists of a colloidal particle confined to a narrow optical ring trap, generated via a spatial light modulator (SLM) that sculpts the laser intensity profile into a circular minimum in the horizontal $x - y$ plane. This provides strong radial confinement while allowing free azimuthal motion, effectively localizing the particle to a ring of radius R immersed in water (see Fig. 1).

To break thermal equilibrium and introduce direction-dependent noise, a stochastic electric field $E_y(t)$ is applied along the y-axis using a pair of microelectrodes embedded on opposite sides of the sample. The electrodes are driven by a white-noise voltage source, creating a high-frequency, band-limited fluctuating field that couples to the charged particle. This mimics an effective hot thermal bath along y by enhancing stochastic forcing in that direction. In contrast, the ambient aqueous environment maintains a lower effective temperature along x. The resulting anisotropy $T_y > T_x$, combined with circular confinement, drives the system into a genuine nonequilibrium steady state exhibiting persistent circulating probability currents.

Beyond optical ring traps, similar radial confinements can be realized magnetically using Bloch-wall domain traps in ferrite-garnet films, as demonstrated by Tierno et al.[38]. In that work, paramagnetic nanoparticles are stably confined within circular magnetic bubbles that generate an effectively harmonic radial potential with tunable stiffness, while the particles remain free to diffuse tangentially along the ring. These shell-like cluster states closely resemble our isotropic ring geometry and could therefore provide an alternative experimental platform for Brownian gyrators beyond optical confinement. Importantly, the Bloch-wall traps operate under isotropic thermal conditions, so implementing anisotropic heat baths in such magnetic systems would be a natural next step toward realizing the quadrupolar fluxes predicted here.

Probability density and flux structure

To characterize the non-equilibrium steady state established by anisotropic thermal driving in a ring trap, we analyze the stationary probability distribution and associated probability currents. Unlike planar Brownian gyrators, where fluxes can form simple rotational loops, the ring geometry imposes a strong radial confinement that fundamentally reshapes both the spatial distribution and the flux topology. In this quasi-one-dimensional setting, the angular direction remains free, but the anisotropic diffusion induces a rich angular modulation and persistent circulating currents. The resulting structure reflects a delicate interplay between confinement strength, thermal anisotropy, and spatial geometry.

To derive the steady-state probability distribution $P(r, \theta)$ analytically, we solve the Fokker-Planck equation, given in Eq. (2) and Eq. (3), in the narrow-ring limit. Our calculational strategy begins with an ansatz that separates the leading-order radial confinement from an angular modulation induced by the thermal anisotropy

$$P(r, \theta) = P_0(r, \theta)\ \exp[-\alpha g(r) \cos(2\theta)], \tag{4}$$

where

$$P_0(r, \theta) = \frac{1}{\sqrt{T_r(\theta)}} \exp\left[-\frac{k(r - R)^2}{2T_r(\theta)}\right], \tag{5}$$

is the base distribution for a ring with a locally Gaussian radial profile of width $\sqrt{T_r(\theta)/k}$, and the effective radial temperature $T_r(\theta) = T(1 - \alpha \cos 2\theta)$. The function $g(r)$ captures the first-order correction due to anisotropic noise encoded in the anisotropy parameter α.

Substituting this ansatz into the steady-state Fokker-Planck equation and expanding to linear order in the anisotropy parameter α yields an ordinary differential equation for $g(r)$ (see SM). We solve this equation perturbatively in the narrow-ring limit by expanding $g(r)$ around the trap minimum $r = R$ as a second-order polynomial, $g(R + \rho) \approx a_0 + a_1\rho + a_2\rho^2$, where $\rho = r - R$. Matching terms order-by-order determines the coefficients a_1 and a_2, leading to our final expression for the steady-state probability

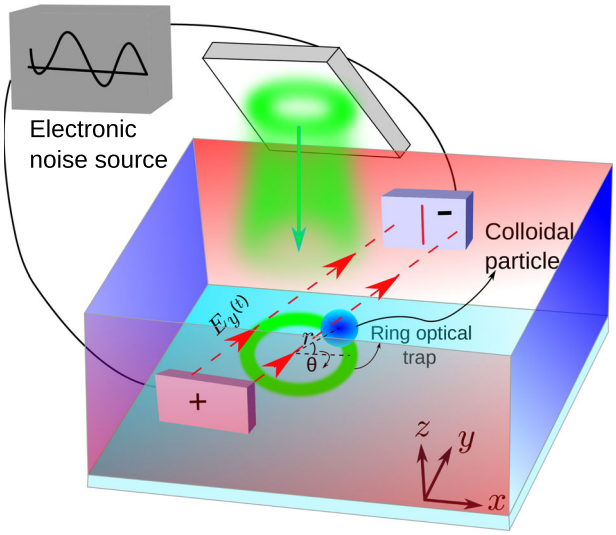

Fig. 1 | Schematic illustration of the model and a potential experimental realization. A colloidal particle (blue) is confined within a ring-shaped optical trap generated via a spatial light modulator. Anisotropic thermal noise is introduced by applying a fluctuating electric field $E_y(t) \sim$ white noise along the y-direction using a pair of electrodes placed on opposite sides of the trap along y. This creates an effective hot bath along y, while the ambient aqueous medium provides a colder bath along x. Note that the system is two-dimensional, and the three-dimensional schematic is for clarity of illustration.

density, which reads

$$P(\rho,\theta) \approx \frac{1}{\mathcal{N}\sqrt{T_r(\theta)}} \exp\left[-\frac{k\rho^2}{2T_r(\theta)} - \alpha\left(a_1\rho + a_2\rho^2\right)\cos(2\theta)\right], \quad (6)$$

where $\mathcal{N} \approx 2\pi R\sqrt{2\pi/k}$ is the normalization constant. The geometric coefficients appearing in the angular modulation are given by $a_1 = (2kR^2 - 4T)/(kR^3 + RT)$ and $a_2 = (-2kR^2 + T)/(kR^4 + R^2T)$. The key feature of this expression is the angular modulation of the density, which breaks rotational symmetry and encodes the directionality of fluxes. The radial and angular fluxes can be calculated using the probability density in Eq. (6) as shown in Methods and SM.

As shown in Fig. 2, the steady-state density forms a sharply localized ring around $r = R$, consistent with the imposed confinement. The modulation along θ is subtle but discernible, reflecting the influence of anisotropic diffusion. The associated flux field, shown in both polar and Cartesian representations (Figs. 2–3), exhibits a striking quadrupolar pattern. Radial fluxes, inward and outward (Fig. 2b, e), coexist with angular circulations (Fig. 2c, f), generating a coherent vortex structure. The full streamline plots (Fig. 3) highlight this behavior, with extended vortical loops for larger R, and more compact, tightly wound recirculations for smaller R. This transition indicates enhanced localization and stronger angular anisotropy at small radii, illustrating how trap geometry governs the qualitative features of the steady state.

In Fig. 4, we present a direct quantitative comparison between the analytical predictions and Brownian dynamics simulations (see Methods) for several temperature anisotropy ratios $\beta = T_y/T_x$. The angular profile of the probability density $P(R, \theta)$ and the radial flux components $J_r(r, 0)$ and $J_\theta(r, \pi/4)$ exhibit excellent agreement for moderate anisotropies ($\beta \leq 2.0$),

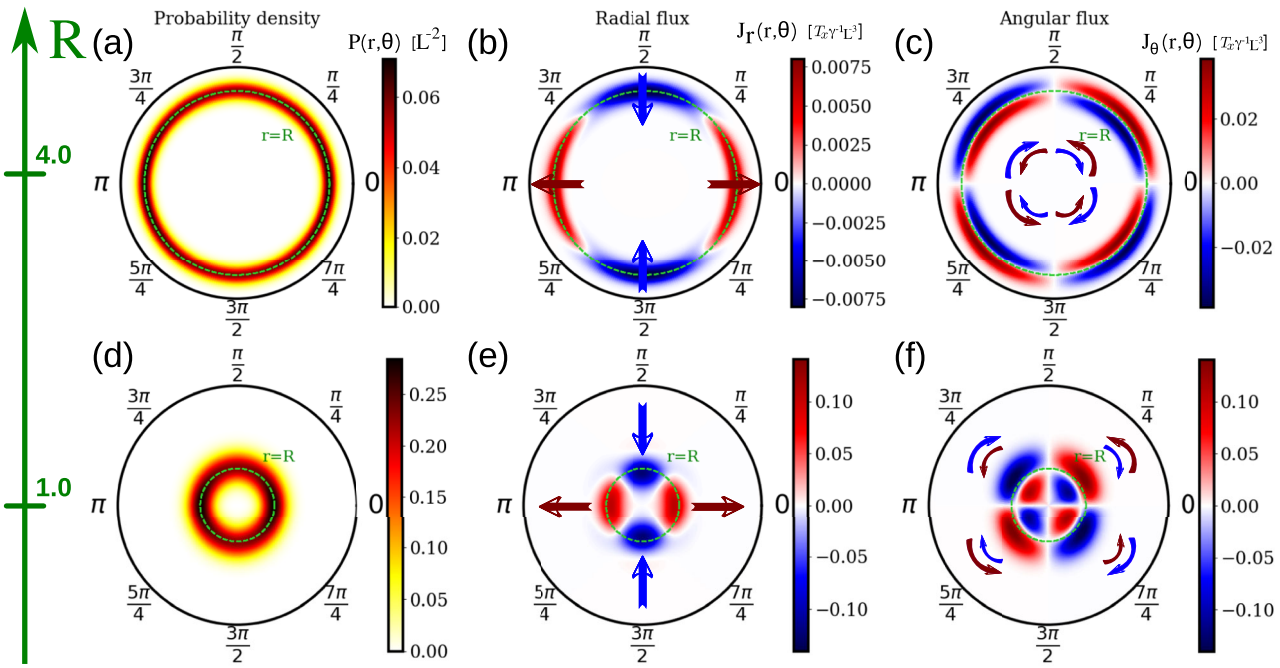

Fig. 2 | Theory: Steady-state probability density and probability flux components. a–c Correspond to $R = 4.0$, while (**d–f**) show $R = 1.0$. In all cases, the trap stiffness is $k = 20$, and the temperature ratio $\beta = 1.5$, with characteristic length scale $L = \sqrt{T_x/k}$. **a**, **d** The probability distribution, plotted from Eq. (6), is sharply localized around the ring $r = R$ (indicated by dashed circles), and anisotropic thermal noise induces an angular modulation visible as slight distortions along the θ-direction. **b**, **e** The radial flux, plotted from Eq. (14), highlights the local circulating currents that maintain the non-equilibrium steady state. Inward and outward flow regions are indicated by blue and dark-red straight arrows, respectively, illustrating the direction of radial motion. **c**, **f** The angular flux from Eq. (15), emphasizes the sustained azimuthal circulating motion characteristic of gyrators. Blue and dark-red curved arrows indicate clockwise and counter-clockwise circulations, respectively. For $R = 4.0$ (top row), the probability density forms a broad annulus with smoother flux patterns, indicating a more delocalized state. In contrast, for $R = 1.0$ (bottom row), the probability is tightly localized and the flux components are more concentrated, highlighting stronger confinement and enhanced rotational features. The dashed circles at $r = R$ serve as a reference to the nominal ring radius and emphasize the degree of spatial localization.

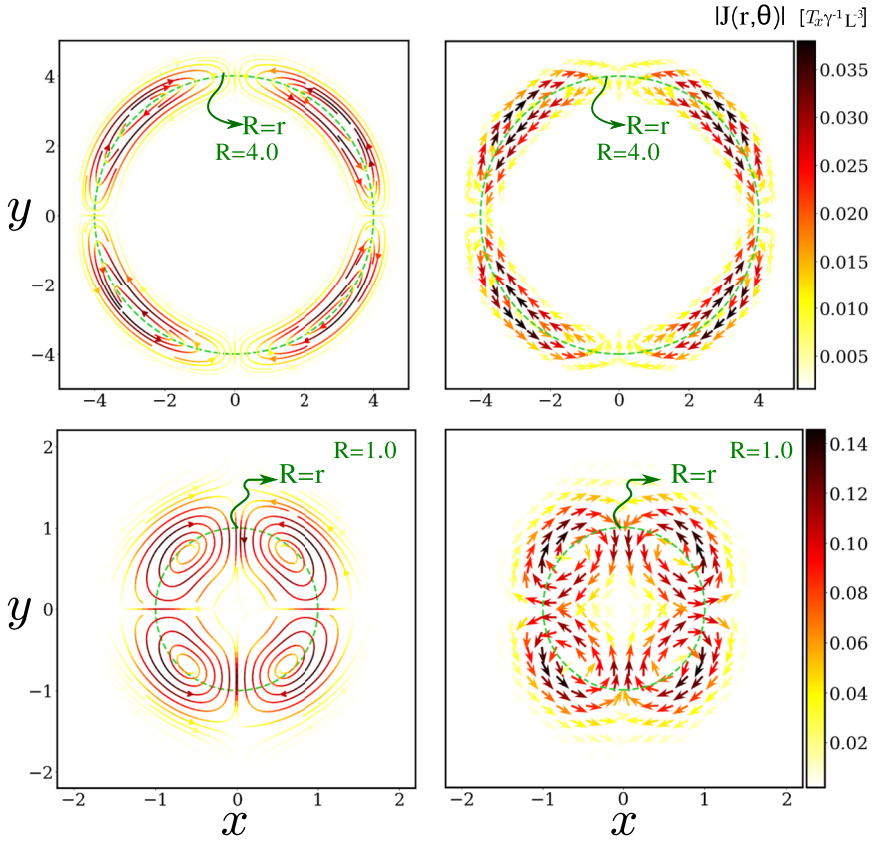

Fig. 3 | Theory: Probability flux streamlines and quiver plots. Top panels correspond to $R = 4.0$, bottom panels to $R = 1.0$. The steady-state probability flux $\mathbf{J}(r, \theta)$ is projected in Cartesian coordinates (x, y), with streamlines visualizing circulation patterns and quiver arrows indicating local flux directions. Color maps encode the flux magnitude $|\mathbf{J}(r, \theta)|$ for $\beta = 1.5$ and $k = 20$, with $L = \sqrt{T_x/k}$. For $R = 4.0$ (top), the flux forms extended vortex-like loops, while for $R = 1.0$ (bottom), circulation becomes more localized with pronounced radial and azimuthal components due to tighter confinement and stronger anisotropy. Green dashed circles mark the nominal ring position $r = R$. Results computed directly from Eqs. (14), (15).

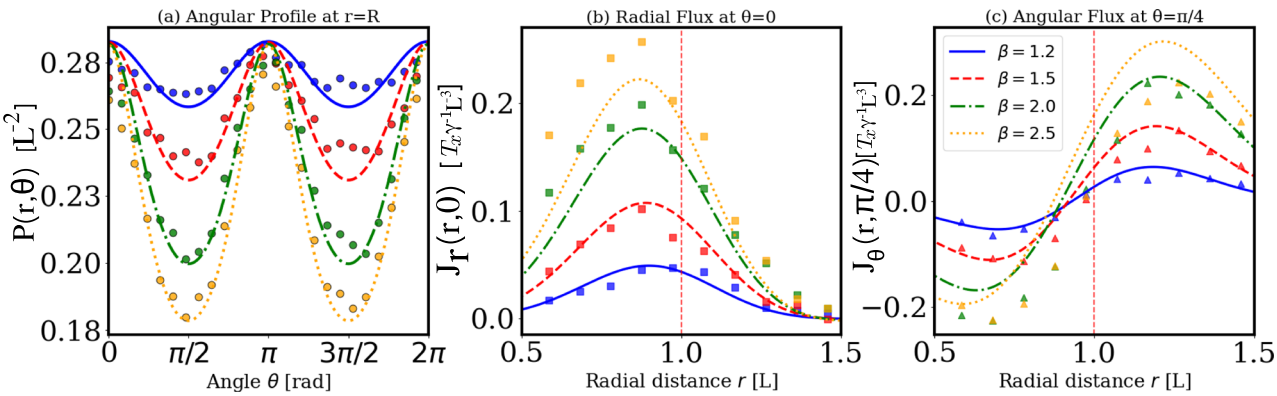

Fig. 4 | Quantitative comparison between analytical theory and simulations. **a** Angular profile of the steady-state probability density $P(R, \theta)$ at the ring radius $r = R$ with characteristic length scale $L = \sqrt{T_x/k}$. **b** Radial dependence of the radial flux component $J_r(r, \theta = 0)$ along the x-axis. **c** Radial dependence of the angular flux component $J_\theta(r, \theta = \pi/4)$. Solid lines denote analytical predictions from Eqs. (6) and (14)–(15), while symbols represent results from Brownian dynamics simulations. Colors correspond to temperature ratios $\beta = T_y/T_x = 1.2$ (blue), 1.5 (red), 2.0 (green), and 2.5 (orange). Excellent agreement is observed for $\beta \leq 2.0$, validating the perturbative analytical approach, whereas deviations at $\beta = 2.5$ mark the onset of nonlinear effects beyond the linear-order theory. In all cases, the trap stiffness is $k = 20$ and $R = 1.0$.

confirming the predictive accuracy of the perturbative analytical solution in the narrow-ring limit. For stronger anisotropy ($\beta = 2.5$), small systematic deviations appear, indicating the onset of nonlinear effects beyond the linear-order expansion.

Entropy production density

We now quantify local irreversibility in the non-equilibrium steady state, by evaluating the spatially resolved entropy production density[39–42] $\sigma(r, \theta)$, defined as $\sigma(r, \theta) = \mathbf{J}^\top \mathbf{D}^{-1} \mathbf{J}/P(r, \theta)$, where $\mathbf{J}$ is the steady-state flux, $\mathbf{D}$ is the diffusion tensor in Eq. (3), and $P(r, \theta)$ is the steady-state probability density as in Eq. (6). In our system, this quantity admits an explicit analytic expression under the narrow-ring approximation due to the constant determinant of $\mathbf{D}$ (see SM). The result exhibits a pronounced quadrupolar angular modulation through $\cos^2(2\theta)$ and $\sin^2(2\theta)$ terms, modulated by a radial Gaussian envelope centered around the trap minimum $r = R$.

The radial entropy production profile $\sigma(r)$, obtained via angular averaging, reveals a non-monotonic structure that depends sensitively on the ring radius R (Fig. 5). For larger rings, entropy production spreads broadly along the radial direction, while smaller rings concentrate dissipation more sharply near the center. In both cases, $\sigma(r)$ develops symmetric off-centered peaks and can exhibit a suppression at $r = R$, despite the maximum of the probability density there. This counterintuitive dip reflects

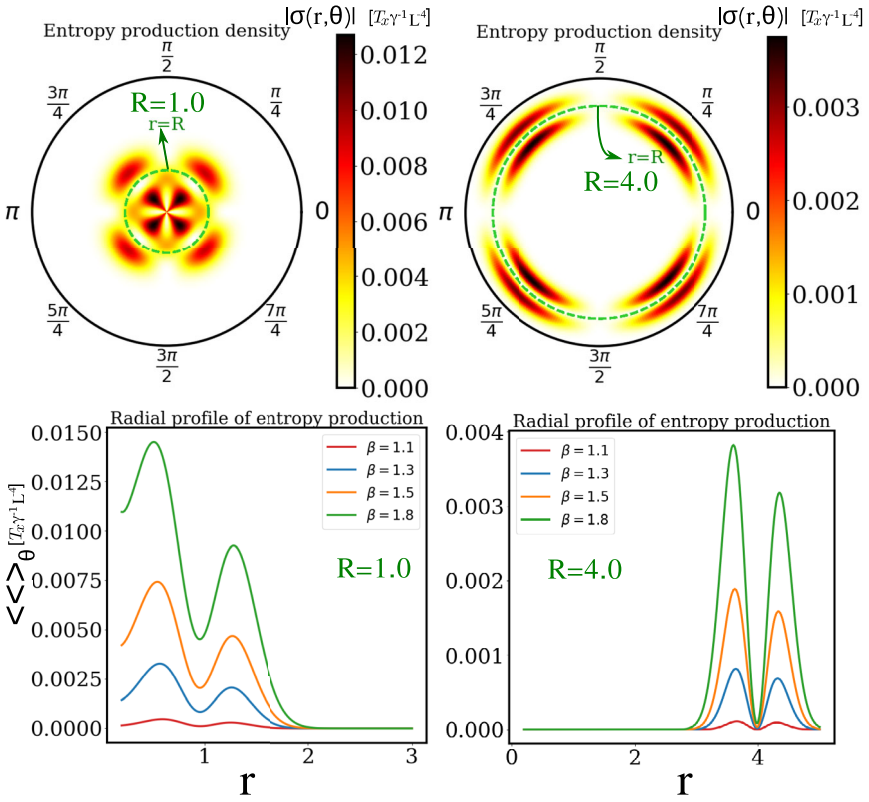

Fig. 5 | Theory: Entropy production density and radial profiles. Top: Steady-state entropy production density $|\sigma(r,\theta)|$ plotted in polar coordinates for two ring radii, $R = 1.0$ (left) and $R = 4.0$ (right). System parameters are $k = 20$, $\beta = 1.5$, and characteristic length scale $L = \sqrt{T_x/k}$. The dashed green circle denotes the nominal trap location $r = R$. For the smaller radius, dissipation is strongly concentrated near the center, forming localized hot spots due to enhanced angular modulation and curvature effects. In contrast, for the broader ring, entropy production becomes more azimuthally extended and radially delocalized, forming a narrow quadrupolar band. Bottom: Radial profiles of the angularly averaged entropy production $\langle\sigma(r,\theta)\rangle_\theta$ for varying anisotropy $\beta = T_y/T_x$, shown for both trap sizes. Increasing β amplifies the overall dissipation and shifts it outward, consistent with enhanced rotational driving. All curves exhibit non-monotonic structure with symmetric off-centered peaks around the trap minimum, reflecting the geometric suppression of flux at $r = R$. Results obtained from the analytical expressions Eq. (18) and Eq. (19).

the vanishing of radial flux and the geometric modulation of angular currents near the trap minimum. The overall amplitude of $\sigma(r)$ scales as α^2, underscoring that irreversibility emerges purely from the imposed anisotropic fluctuations.

Quadrupolar gyration

The emergence of quadrupolar circulation in the ring Brownian gyrator arises from the interplay between confinement geometry and anisotropic thermal noise. Although the particle is confined to a rotationally symmetric ring, the projection of the diffusion anisotropy onto the local polar basis introduces an effective angular modulation of noise. Specifically, the effective temperatures in the radial and angular directions vary with position as $T_r(\theta) = T(1 - \alpha\cos(2\theta))$ and $T_\theta(\theta) = T(1 + \alpha\cos(2\theta))$. This spatial variation in local diffusivity generates alternating thermodynamic forces along the ring, leading to localized circulating currents in the steady state.

The underlying diffusion tensor, given in Eq. (3), has eigenvalues $\lambda_- = T_x$ and $\lambda_+ = T_y$, corresponding to the directions of minimal (cold) and maximal (hot) axis, respectively. While the eigenvalues are uniform, the associated eigenvectors rotate continuously along the ring: the hot axis points along $\mathbf{v}_{\rm hot}(\theta) = (\sin\theta, \cos\theta)$, while the cold axis lies along $\mathbf{v}_{\rm cold}(\theta) = (\cos\theta, -\sin\theta)$. In polar coordinates, the hot axis is locally aligned with angle $\phi = \theta$, and the cold axis with $\phi = -\theta$, indicating a continuously rotating anisotropy tied to the particle's position.

This spatially rotating anisotropy breaks detailed balance and induces a structured non-equilibrium current pattern, as illustrated in Fig. 6. The ring can be heuristically viewed as partitioned into four quadrants, each effectively acting as a local Brownian gyrator. In each region, the radial confinement projects the anisotropic fluctuations into misaligned geometric directions, generating alternating clockwise and counterclockwise circulating fluxes that collectively form the global quadrupolar pattern.

To quantify the strength of the four alternating local circulation, we introduce a scalar *quadrupolarity amplitude* $Q_{\rm amp}$, defined as the magnitude of the $m = 2$ Fourier component of the tangential flux $J_\theta(R,\theta)$ obtained from Eq. (15). The quadrupolarity amplitude reads (see Supplementary Material)

$$Q_{\rm amp} = \frac{\mu\,\alpha\,\sqrt{kT}}{4\sqrt{2}\,\pi^{3/2}\,R^2}. \tag{7}$$

This quantity measures the amplitude of the characteristic four-cell circulation and grows linearly with the thermal anisotropy α, vanishing in the isotropic limit. In our convention ($\alpha > 0$), $Q_{\rm amp} > 0$, providing a compact scalar descriptor of the non-equilibrium circulation that complements the full spatial flux maps. A value $Q_{\rm amp} = 1$ would indicate a purely quadrupolar $\sin(2\theta)$ mode, while smaller values reflect admixtures of higher harmonics or imperfect symmetry.

Discussion

Our study reveals how spatial confinement and thermal anisotropy can conspire to generate intricate nonequilibrium dynamics in an otherwise force-free, passive system. By coupling a Brownian particle to orthogonal heat baths within a ring-shaped trap, we uncover a robust mechanism for producing quadrupolar probability currents and structured entropy production—without invoking self-propulsion, external fields, or interactions. The ring geometry plays a central role, transforming what would otherwise be linear or planar transport into circulating steady-state motion characterized by symmetry breaking and vorticity inversion.

Unlike planar Brownian gyrators, where rotation emerges from the misalignment of the potential axes relative to anisotropic noise, the ring geometry considered here preserves isotropic radial confinement. The fixed Cartesian anisotropy of the baths projects onto the tangential direction as a $cos(2\theta)$ modulation of the local diffusivity. This spatial modulation breaks continuous rotational symmetry and results in a steady-state flux field with four alternating gyrating sectors, i.e., quadrupolar gyration, and entropy production patterns that are highly localized yet globally balanced. Our analytical treatment captures these features in the narrow-ring limit and to leading order in the temperature anisotropy, while simulations confirm their persistence across a broader range of parameters.

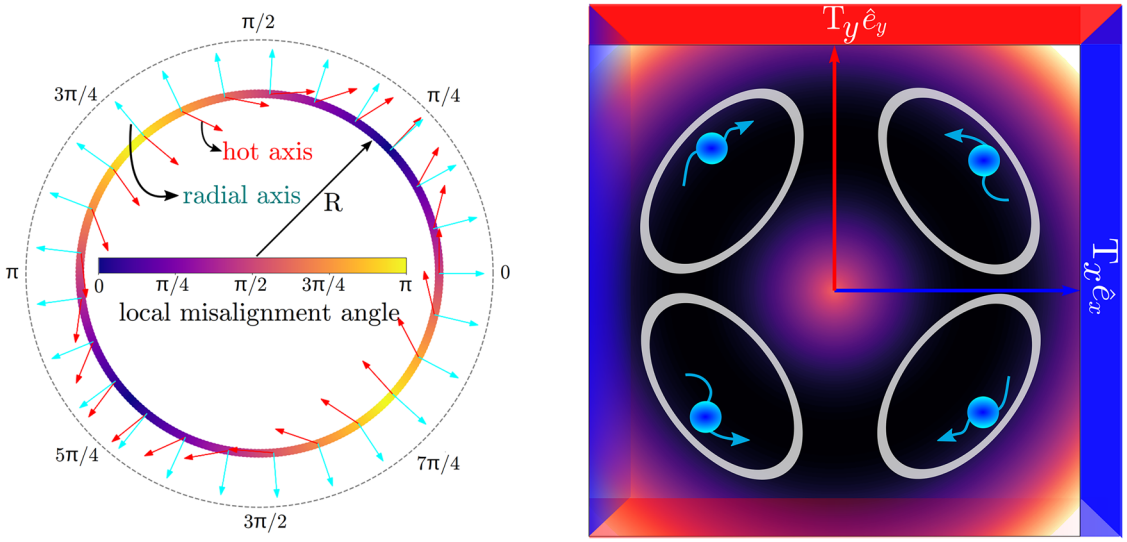

Fig. 6 | Quadrupolar flux structure from locally rotating hot axes. (Left) Visualization of the local misalignment angle (color) between the radial direction and the hot axis of anisotropic diffusion as a function of position along the ring. Blue and red arrows represent the cold and hot diffusion directions, respectively, highlighting the continuous spatial rotation of the anisotropic diffusion tensor. (Right) Schematic representation of the resulting quadrupolar current pattern: the ring can be heuristically decomposed into four quadrants, each behaving as an effective Brownian gyrator with locally projected anisotropy. The angular variation of the hot axis generates alternating clockwise (CW) and counterclockwise (CCW) circulating fluxes, collectively forming a robust quadrupolar current structure in the steady state.

Beyond its theoretical significance, our model offers a versatile framework for designing stochastic thermal machines[43] where geometry and temperature anisotropy govern microscopic motion[44]. It opens avenues for exploring fluctuation-driven organization[45] in confined colloidal systems[46–50] including active matter[51,52], with implications for microrheology, multi-terminal stochastic heat engines[53], transport in curved environments[54], and synthetic engines. Our findings provide a basis for exploring coupled ring gyrators to explore collective flux organization and energy transfer, which could lead to synchronization, phase-locking, or emergent collective currents. Future directions include designing optimal loading protocols for work extraction and exploring whether similar quadrupolar flux patterns can arise in chiral (passive or active) particles with spatially varying handedness.

Methods

Theoretical predictions

We analytically characterize the non-equilibrium steady state of a Brownian particle confined in a narrow ring and subject to anisotropic thermal fluctuations. The system is described by the time-dependent Fokker–Planck equation in polar coordinates (r, θ), which governs the evolution of the probability density $P(r, \theta, t)$. The dynamics involve coordinate-dependent drift and diffusion due to both confinement and the angular dependence of the diffusion tensor induced by temperature anisotropy.

As derived in the SM, the time-dependent Fokker–Planck equation takes the divergence form

$$\partial_t P(r,\theta,t) = -\frac{1}{r}\frac{\partial}{\partial r}\left[rJ_r(r,\theta,t)\right] - \frac{1}{r}\frac{\partial}{\partial\theta}J_\theta(r,\theta,t), \tag{8}$$

where the flux components J_r and J_θ follow from direct projection of the anisotropic Cartesian flux onto the polar basis, which read (see SM for full derivation)

$$J_r = -\mu k(r-R)P - D_r(\theta)\frac{\partial P}{\partial r} - \frac{D_{r\theta}(\theta)}{r}\frac{\partial P}{\partial\theta}, \tag{9}$$

$$J_\theta = -D_{r\theta}(\theta)\frac{\partial P}{\partial r} - \frac{D_\theta(\theta)}{r}\frac{\partial P}{\partial\theta}, \tag{10}$$

with the angle-dependent diffusion coefficients defined as

$$D_r(\theta) = \mu T(1-\alpha\cos(2\theta)), \tag{11}$$

$$D_\theta(\theta) = \mu T(1+\alpha\cos(2\theta)), \tag{12}$$

$$D_{r\theta}(\theta) = \mu T\alpha\sin(2\theta), \tag{13}$$

where μ is the mobility, $\alpha = (\beta-1)/(\beta+1)$ is the dimensionless anisotropy parameter and $T = T_x(\beta+1)/2$ is the mean effective temperature with $\beta = T_y/T_x$ where $\beta = 1$ corresponds to the isotropic system. All stochastic differential equations are interpreted in the Itô sense with additive Cartesian noise[36,37]. The transformation to polar coordinates is carried out only at the level of the Fokker–Planck equation, so that the coordinate change is purely kinematic and automatically incorporates the geometric divergence term without generating any additional noise-induced drift.

To make analytical progress, we perform a perturbative expansion valid in the narrow-ring limit around $r = R$. Retaining terms only linear in the anisotropy parameter α, we obtain approximate expressions for the steady-state probability flux components:

$$J_r(r,\theta) \approx \frac{\alpha\mu\sqrt{kT}\,e^{-\frac{k(r-R)^2}{2T}}}{(2\pi)^{3/2}R}\left(a_1 + 2a_2(r-R)\right)\cos(2\theta), \tag{14}$$

$$J_\theta(r,\theta) \approx \frac{\alpha\mu\sqrt{k}\,e^{-\frac{k(r-R)^2}{2\mu T}}}{\sqrt{T}(2\pi)^{3/2}Rr}\left(T + (r-R)\left[kR - 2(a_1 + a_2(r-R))T\right]\right)\sin(2\theta). \tag{15}$$

where the coefficients a_1 and a_2 depend only on k, R, and T, and are given by:

$$a_1 = \frac{2kR^2 - 4T}{kR^3 + RT}, \tag{16}$$

$$a_2 = \frac{-2kR^2 + T}{kR^4 + R^2T}. \tag{17}$$

These expressions capture the emergence of quadrupolar structure in the steady-state fluxes, driven solely by anisotropic fluctuations in a rotationally symmetric trap. In this limit, the probability density remains approximately Gaussian in the radial direction, while the angular modulation of the fluxes generates circulating currents that break detailed balance. This perturbative framework provides a controlled route to predicting flux patterns, entropy production, and irreversibility in confined nonequilibrium systems.

At leading order in the narrow-ring limit, the steady-state probability and flux fields admit approximate analytical expressions, yielding a closed-form for the local entropy production density

$$\sigma(r,\theta) = \frac{\alpha^2 e^{-\frac{k(r-R)^2}{2T}}\sqrt{k}\mu}{4\sqrt{2}\pi^3 T^{3/2}(R-R\alpha^2)}\left[\left(a_1+2a_2(r-R)\right)^2 T^2\cos^2(2\theta) + \frac{\left(T+(r-R)\left(kR-2(a_1+a_2(r-R))T\right)\right)^2\sin^2(2\theta)}{r^2}\right], \tag{18}$$

which exhibits a pronounced quadrupolar angular structure encoded by $\cos^2(2\theta)$ and $\sin^2(2\theta)$ modulations, and a radial Gaussian envelope centered around $r = R$.

The corresponding radial profile, obtained by angular averaging, reads

$$\sigma(r) = \frac{\alpha^2 e^{-\frac{k(r-R)^2}{2T}}\sqrt{k}\mu}{8\sqrt{2}\pi^4 T^{3/2}(R-R\alpha^2)}\left[\pi(a_1+2a_2(r-R))^2 T^2 + \frac{\pi\left(T+(r-R)(kR-2(a_1+a_2(r-R))T)\right)^2}{r^2}\right], \tag{19}$$

revealing nontrivial radial dependence with peaks that shift and grow with increasing anisotropy α. The amplitude of $\sigma(r)$ scales as α^2, highlighting that entropy production is entirely driven by the imposed temperature gradient. This structure reflects the interplay between geometric confinement, flux topology, and anisotropic fluctuations.

Marginal angular probability distribution

To connect the two-dimensional steady-state probability density $P(r,\theta)$ with experimentally accessible observables, we evaluate its angular marginal obtained by integrating over the radial coordinate,

$$P_\theta(\theta) = \int_0^\infty r\,P(r,\theta)\,dr. \tag{20}$$

Using the analytical steady-state solution, Eq. (6), and valid in the narrow-ring limit, the integration can be performed explicitly. For a strongly confined particle ($\sqrt{T/k} \ll R$), the result reads (see SM for details)

$$P_\theta(\theta) \simeq \frac{1}{2\pi}[1+\alpha\,\Gamma\,\cos(2\theta)],\ \Gamma = \frac{T(2kR^2-T)}{kR^2(kR^2+T)}, \tag{21}$$

where $\Gamma = \mathcal{O}(\varepsilon^2)$ with $\varepsilon = \sqrt{T/k}/R$ quantifies the relative ring width. In the asymptotic limit $kR^2/T \gg 1$, this reduces to $\Gamma \simeq 2\varepsilon^2$, showing that the anisotropy-induced modulation is suppressed quadratically with the ring width. The steady state remains nearly uniform around the ring, but exhibits a weak $\cos(2\theta)$ modulation of relative amplitude $\alpha\Gamma$. This small deviation from isotropy arises from the coupling between the angularly dependent diffusivity and the finite radial extent of the ring. In the razor-thin limit ($\varepsilon \to 0$), the modulation vanishes and $P_\theta(\theta)$ becomes strictly uniform.

The marginal angular distribution $P_\theta(\theta)$ provides a direct experimental observable. From particle trajectories $\theta(t)$ recorded in an optical or magnetic ring trap, one can construct the stationary histogram $P_\theta(\theta)$ and fit it to

$$P_\theta(\theta) \simeq \frac{1}{2\pi}\left[1+\alpha_{\text{eff}}\cos(2\theta-\phi_0)\right], \tag{22}$$

where ϕ_0 identifies the orientation of the anisotropy axis in the laboratory frame, and $\alpha_{\text{eff}} = \alpha\Gamma$ quantifies the effective strength of thermal anisotropy. The predicted scaling $\Gamma = O(\varepsilon^2)$ implies that the modulation is subtle but measurable for moderate ring widths or sufficiently strong anisotropy ratios (T_y/T_x), thus providing a simple experimental test of the theory.

Numerical simulations

To verify our analytical predictions, we also perform Brownian dynamics simulations of the system. The dynamics of the particle's position $\boldsymbol{r}(t) = (x(t), y(t))$ can be described by the following overdamped Langevin equation

$$\dot{\boldsymbol{r}} = -\mu\nabla U(r) + \boldsymbol{\xi}(t) \tag{23}$$

where μ is the mobility, $\boldsymbol{\xi}(t) = (\xi_x(t), \xi_y(t))$ is a Gaussian white noise vector with zero mean and $\langle\eta_i(t)\eta_j(t')\rangle = 2\mu T_i\delta_{ij}\delta(t-t')$ where $i,j \in \{x,y\}$

The simulations are performed using an Euler-Maruyama integration scheme with a discrete time step $dt = 1\times10^{-3}\gamma/k$, chosen to be sufficiently small to ensure numerical stability and accuracy. Thermal noise is implemented by drawing random numbers from a normal distribution at each time step.

All theoretical predictions have been cross-validated against Brownian dynamics simulations, as shown in the main text (see Fig. 4) and in the Supplementary Material. In the narrow-ring regime, where the analytical approach is well-controlled, we find excellent agreement.

Data availability

The simulation data used to generate Figure~4 in the main text and all figures in the Supplementary Material are available at https://doi.org/10.5281/zenodo.17609030.

Code availability

The code to reproduce Fig. 4 is updated to a public repository at the link Zenodo: https://doi.org/10.5281/zenodo.17609030and is available from I.A., the corresponding author, upon request.

Received: 12 August 2025; Accepted: 30 December 2025;
Published online: 03 March 2026

References

1. Filliger, R. & Reimann, P. Brownian gyrator: A minimal heat engine on the nanoscale. *Phys. Rev. Lett.* **99**, 230602 (2007).
2. Ciliberto, S., Imparato, A., Naert, A. & Tanase, M. Heat flux and entropy produced by thermal fluctuations. *Phys. Rev. Lett.* **110**, 180601 (2013).
3. dos S Nascimento, E. & Morgado, W. A. Stationary properties of a non-markovian brownian gyrator. *J. Stat. Mech.: Theory Exp.* **2021**, 013301 (2021).
4. Movilla Miangolarra, O., Taghvaei, A., Fu, R., Chen, Y. & Georgiou, T. T. Energy harvesting from anisotropic fluctuations. *Phys. Rev. E* **104**, 044101 (2021).
5. Squarcini, A., Solon, A., Viot, P. & Oshanin, G. Fractional brownian gyrator. *J. Phys. A: Math. Theor.* **55**, 485001 (2022).
6. Cerasoli, S. et al. Spectral fingerprints of nonequilibrium dynamics: the case of a brownian gyrator. *Phys. Rev. E* **106**, 014137 (2022).
7. Siches, J. V., Miangolarra, O. M., Taghvaei, A., Chen, Y. & Georgiou, T. T. Inertialess gyrating engines. *PNAS nexus* **1**, pgac251 (2022).
8. Miangolarra, O. M., Taghvaei, A., Chen, Y. & Georgiou, T. T. Thermodynamic engine powered by anisotropic fluctuations. *Phys. Rev. Res.* **4**, 023218 (2022).
9. Abdoli, I., Sommer, J.-U., Löwen, H. & Sharma, A. Escape dynamics in an anisotropically driven brownian magneto-system. *Europhys. Lett.* **139**, 21003 (2022).

10. Miangolarra, O. M. Energy harvesting from anisotropic temperature fields. In *Stochastic Thermodynamic Treatment of Thermal Anisotropy*, 51–79 (Springer, 2024).
11. Miangolarra, O. M., Taghvaei, A. & Georgiou, T. T. Minimal entropy production in the presence of anisotropic fluctuations. In *IEEE Transactions on Automatic Control* (2024).
12. Miangolarra, O. M. Stochastic thermodynamic systems subject to anisotropic fluctuations. In *Stochastic Thermodynamic Treatment of Thermal Anisotropy*, 39–50 (Springer, 2024).
13. Chiang, K.-H., Lee, C.-L., Lai, P.-Y. & Chen, Y.-F. Electrical autonomous brownian gyrator. *Phys. Rev. E* **96**, 032123 (2017).
14. Pietzonka, P. & Seifert, U. Universal trade-off between power, efficiency, and constancy in steady-state heat engines. *Phys. Rev. Lett.* **120**, 190602 (2018).
15. Bae, Y., Lee, S., Kim, J. & Jeong, H. Inertial effects on the brownian gyrator. *Phys. Rev. E* **103**, 032148 (2021).
16. Seifert, U. Stochastic thermodynamics, fluctuation theorems and molecular machines. *Rep. Prog. Phys.* **75**, 126001 (2012).
17. Dotsenko, V., Maciołek, A., Vasilyev, O. & Oshanin, G. Two-temperature Langevin dynamics in a parabolic potential. *Phys. Rev. E* **87**, 062130 (2013).
18. Koyuk, T. & Seifert, U. Thermodynamic uncertainty relation for time-dependent driving. *Phys. Rev. Lett.* **125**, 260604 (2020).
19. Leighton, M. P., Ehrich, J. & Sivak, D. A. Information arbitrage in bipartite heat engines. *Phys. Rev. X* **14**, 041038 (2024).
20. Abdoli, I. et al. Correlations in multithermostat brownian systems with Lorentz force. *N. J. Phys.* **22**, 093057 (2020).
21. Abdoli, I. et al. Tunable brownian magneto heat pump. *Sci. Rep.* **12**, 13405 (2022).
22. Muhsin, M., Adersh, F. & Sahoo, M. Active magneto gyrator: Memory-induced trapped diamagnetism. *Phys. Rev. E* **111**, 015411 (2025).
23. Adersh, F., Muhsin, M. & Sahoo, M. Active magneto gyrator as a tunable heat engine or heat pump. *Phys. Rev. E* **112**, 025416 (2025).
24. Chang, H., Lee, C.-L., Lai, P.-Y. & Chen, Y.-F. Autonomous brownian gyrators: a study on gyrating characteristics. *Phys. Rev. E* **103**, 022128 (2021).
25. Das, B., Manikandan, S. K. & Banerjee, A. Inferring entropy production in anharmonic brownian gyrators. *Phys. Rev. Res.* **4**, 043080 (2022).
26. Argun, A. et al. Experimental realization of a minimal microscopic heat engine. *Phys. Rev. E* **96**, 052106 (2017).
27. Abdoli, I., Sharma, A. & Löwen, H. Enhanced efficiency in shear-loaded Brownian gyrators. *Phys. Fluids* **37** (2025).
28. Roichman, Y., Sun, B., Stolarski, A. & Grier, D. G. Influence of nonconservative optical forces on the dynamics of optically trapped colloidal spheres: the fountain of probability. *Phys. Rev. Lett.* **101**, 128301 (2008).
29. Sun, B., Lin, J., Darby, E., Grosberg, A. Y. & Grier, D. G. Brownian vortexes. *Phys. Rev. E—Stat., Nonlinear, Soft Matter Phys.* **80**, 010401 (2009).
30. Saha, D., Tarama, S., Löwen, H. & Egelhaaf, S. U. Cybloids–creation and control of cybernetic colloids. *Soft Matter* **20**, 8112–8124 (2024).
31. Chand, R., Shukla, A. & Kumar, G. P. Optothermal revolution: Colloids in an optical ring trap. *ACS Photonics* **12**, 855–863 (2025).
32. Kundu, A., Comtet, A. & Majumdar, S. N. Winding statistics of a brownian particle on a ring. *J. Phys. A: Math. Theor.* **47**, 385001 (2014).
33. Grange, P. Winding number of a brownian particle on a ring under stochastic resetting. *J. Phys. A: Math. Theor.* **55**, 155003 (2022).
34. Proesmans, K. & Derrida, B. Large-deviation theory for a brownian particle on a ring: a WKB approach. *J. Stat. Mech.: Theory Exp.* **2019**, 023201 (2019).
35. Fazli, Z. & Naji, A. Active particles with polar alignment in ring-shaped confinement. *Phys. Rev. E* **103**, 022601 (2021).
36. Gardiner, C. *Stochastic methods: A Handbook for the Natural and Social Sciences*, 4th edn (Springer, 2009).
37. Lau, A. W. C. & Lubensky, T. C. State-dependent diffusion: thermodynamic consistency and its path integral formulation. *Phys. Rev. E* **76**, 011123 (2007).
38. Tierno, P., Johansen, T. H. & Straube, A. V. Thermally active nanoparticle clusters enslaved by engineered domain wall traps. *Nat. Commun.* **12**, 5813 (2021).
39. Puglisi, A. A brief introduction to the inference of entropy production through the fluctuations of currents. *Europhys. Lett.* **150**, 67001 (2025).
40. Fernandez, L., Hess, S. & Klapp, S. H. Nonequilibrium dynamics and entropy production of a trapped colloidal particle in a complex nonreciprocal medium. *Phys. Rev. E* **109**, 054129 (2024).
41. Cates, M. E., Fodor, É, Markovich, T., Nardini, C. & Tjhung, E. Stochastic hydrodynamics of complex fluids: discretisation and entropy production. *Entropy* **24**, 254 (2022).
42. Loos, S. A. & Klapp, S. H. Heat flow due to time-delayed feedback. *Sci. Rep.* **9**, 2491 (2019).
43. Whitelam, S. Demon in the machine: learning to extract work and absorb entropy from fluctuating nanosystems. *Phys. Rev. X* **13**, 021005 (2023).
44. Rings, D., Chakraborty, D. & Kroy, K. Rotational hot brownian motion. *N. J. Phys.* **14**, 053012 (2012).
45. Manikandan, S. K., Dabelow, L., Eichhorn, R. & Krishnamurthy, S. Efficiency fluctuations in microscopic machines. *Phys. Rev. Lett.* **122**, 140601 (2019).
46. Williams, I., Oğuz, E. C., Bartlett, P., Löwen, H. & Royall, C. P. Direct measurement of osmotic pressure via adaptive confinement of quasi-hard disc colloids. *Nat. Commun.* **4**, 2555 (2013).
47. Antonov, A. P. et al. Controlling colloidal flow through a microfluidic y-junction. *Commun. Phys.* **8**, 165 (2025).
48. Cereceda-López, E., Antonov, A. P., Ryabov, A., Maass, P. & Tierno, P. Overcrowding induces fast colloidal solitons in a slowly rotating potential landscape. *Nat. Commun.* **14**, 6448 (2023).
49. Lutz, C., Kollmann, M. & Bechinger, C. Single-file diffusion of colloids in one-dimensional channels. *Phys. Rev. Lett.* **93**, 026001 (2004).
50. Wei, Q.-H., Bechinger, C. & Leiderer, P. Single-file diffusion of colloids in one-dimensional channels. *Science* **287**, 625–627 (2000).
51. Fodor, É, Jack, R. L. & Cates, M. E. Irreversibility and biased ensembles in active matter: Insights from stochastic thermodynamics. *Annu. Rev. Condens. Matter Phys.* **13**, 215–238 (2022).
52. Dolai, P., Krekels, S. & Maes, C. Inducing a bound state between active particles. *Phys. Rev. E* **105**, 044605 (2022).
53. Netz, R. R. Approach to equilibrium and nonequilibrium stationary distributions of interacting many-particle systems that are coupled to different heat baths. *Phys. Rev. E* **101**, 022120 (2020).
54. Villada-Balbuena, A. et al. Single-file dynamics of colloids in circular channels: time scales, scaling laws and their universality. *Phys. Rev. Res.* **3**, 033246 (2021).

Acknowledgements

This work was funded by the Deutsche Forschungsgemeinschaft (DFG, German Research Foundation) under project number 556762905—AB 1083/1-1.

Author contributions

I.A. and H.L. conceived and conceptualized the research. I.A. did the analytical calculations and performed the numerical simulations. H.L. supervised the research. I.A. wrote the first draft, but both authors discussed and interpreted the results and wrote the final version of the manuscript.

Funding

Open Access funding enabled and organized by Projekt DEAL.

Competing interests
The authors declare no competing interests.

Additional information
Supplementary information The online version contains supplementary material available at https://doi.org/10.1038/s44431-025-00015-4.

Correspondence and requests for materials should be addressed to Iman Abdoli.